IJCRT.ORG ISSN : 2320-2882

INTERNATIONAL JOURNAL OF CREATIVE RESEARCH THOUGHTS (IJCRT)

An International Open Access, Peer-reviewed, Refereed Journal

# Review Of Piezo Hydraulic Motors And Their Applications

[1]V K Sri Murali 1st Author, [2]Gokul Kumar K 2nd Author

[1]Research scholar1st Author, [2]Director and Professor 2nd Author

[1]School of Mechanical Engineering (SMEC) 1st Author,

[1]Vellore Institute of Technology, 1st Author, Vellore, Tamil Nadu, India

**Abstract:** Piezo-hydraulic (motors) actuators are a cutting-edge technology designed and developed for applications such as energy harvesting, precise positioning, and providing a blocking force for directional control valves, among other uses. The objectives of this review are to explore the advancements in piezo-hydraulic actuators, summarise their theoretical and experimental results, and assess their applications in various fields. By combining these results, the article provides a comprehensive overview that could serve as valuable data for future development and research. This review supports other research authors in verifying and utilising this data collection for their research work.

**Index Terms** - Piezo hydraulic, actuators, fluid, piezoelectric, and material.

## I. INTRODUCTION

The Piezo-electric motors and actuators review has already been released in the journals. Still, the review article on piezo-hydraulic actuators has not been released. An investigation of piezo-hydraulic energy harvesters, actuators and pump / micro-pump modelling, fabrication, and experimental. Piezoelectric hydraulic motor and valve based on different hysteretic models have been studied chronologically. A recent study examined the root mean square (RMS) voltage for each connection and the proportional relationship between single-channel and multi-channel power generation, noting a sharp increase in voltage as resistance increased from 2 to 100 KΩ. The findings indicate that parallel configurations of a monolithic piezoelectric disk outperform alternative connection methods. The research further demonstrates that voltage is primarily determined by pulse amplitude rather than static pressure [1]. Since control valves lose power, conventional valve-controlled hydraulic cylinders may not be as efficient. Electro-hydrostatic actuation with separate servomotor-driven pumps provides an alternative. A piezo-pump for sub-100W applications—specifically in aerospace, including landing gear actuators—is presented in the journal paper, and it has been highlighted in this review paper. Using disc-style reed valves that allow for pumping frequencies above 1 kHz, the piezo-pump produces an output of 10–100W. 950V peak-to-peak sine wave excitation is provided via custom power electronics. According to experimental data, the pump operates at 1250 Hz with a flow rate of 2 L/min and more than 30 W of hydraulic power when there is no load. Compact power electronics and high-frequency passive reed valves are important developments. The development of piezo pump technology for More Electric aircraft will advance significantly in the future with an emphasis on multi-cylinder pumps and enhanced reed-valve modelling [2]. The output performance of the newly constructed hybrid actuator was examined. The pulsation rates, $\delta$ at 700 Vp-p and 2 MPa bias pressure are 2.29, 2.08, and 1.78 at 400 Hz, 500 Hz, and 600 Hz, respectively. For a single-acting hybrid actuator under identical circumstances, the pulsation rate is 10.98, 11.05, and 17.12. [3]. In addition to their power density, hydraulic actuators are favoured in heavy lifting applications such as exoskeletons. With an emphasis on a piezo-actuator design that uses a bistable buckling beam to enhance the low strain of piezo materials, this research investigates the application of piezo-ceramics for electrically actuated hydraulic valves. Piezo stack integration, bearing design, and the

snapping needs of the beam are major obstacles. The work describes a method to simulate the buckling beam, build the actuator, and deal with bearing friction [4]. Piezo-actuators are applicable in the design of piezo-hydraulic pumps; however, achieving larger flow rates necessitates higher actuation frequencies. This dependency limits their effectiveness with highly viscous fluids at elevated flow rates [5]. For microfluidic systems, the application of electric fields in microchannels is often favoured over pressure-based flow due to compatibility issues. Patterns of shifting pressure and flow rates remain consistent across single, series, and parallel micropump configurations. Revealing an initial frequency increase followed by a decline. Under identical driving conditions, parallel micropumps yield the highest flow and pressure, in contrast to series micropumps, which produce the lowest rates at elevated frequencies of 200 Hz [6],[8]. A piezoelectric hydraulic linear motor with velocity self-monitoring (PHLMVS) displays a significant correlation between monitored velocity and the A3 sensing voltage at a fixed frequency of 500 Hz, with data fitting between velocity and sensor voltage [7]. The average displacement of the piezoelectric transducer after integration with the pump body is less than before coupling, attributed to the fluid counterforce. Forced vibrations yield lower peak displacements compared to free vibrations. The optimal performance of the micropump is noted with a square driving signal, particularly highlighted at 60 Hz under certain peak driving frequencies [8]. To enhance actuation force, a hybrid actuator combining a double-piezoelectric pump and hydraulic cylinder was developed, with a detailed analysis of element design in linkage and driving mechanisms [9]. The study also represents a novel analysis of valve control methods employing hysteresis correction. Experimental results achieved from a new spool valve actuated by a multi-layer piezoelectric ring bender, with a generalised Prandtl-Ishlinskii model applied to model hysteresis based on experimental data from the prototype [10]. In previous research, a unidirectional hybrid actuator was designed, with an initial blocking power below the expected parameters. Consequently, enhancements were made by eliminating air bubbles and redesigning both the hydraulic cylinder and pump chamber, utilising two types of piezo stacks in the process [11]. The development of hybrid actuators that integrate intelligent material-actuated pumps with hydraulic cylinders underscores the significance of fluid and smart material coupling for overall system performance. This investigation also presents results from 2D and 3D fluid flow simulations in a hybrid actuator prototype designed for aviation applications. The simulations indicated significant losses attributed to three-dimensional factors such as radial fluid acceleration and vortex ring formation in the pumping chamber [12]. Operating a piezo hydraulic actuator at higher pumping frequencies is shown to increase power density; however, successful outcomes rely on a comprehensive understanding of the device's dynamics [13]. The study explores the design of a piezoelectric-hydraulic hybrid actuator stepping at high-frequency pumping applications. While prior studies focused on substantial piezoelectric stacks at lower frequencies, this research emphasises the actuator's performance under low volumetric displacement combined with high pumping frequencies. The initial actuator system design is complete, with various system parameters evaluated to identify optimal geometric and piezo-stack characteristics for a specific external load [14].

## II. Piezo Hydraulic Actuators

### 2.1. Hydraulic Piezoelectric Material-Energy Harvester

A new symmetrical hydraulic piezoelectric energy harvester. By combining theoretical analysis, simulation, and empirical testing, the study investigates the energy-harvesting potential of mono-lithic single-side output, monolithic two-side parallel-connected output, stacked one-side parallel-connected output, and stacked two-side parallel-connected output under various parameter configurations.

**Table 1:** Material properties of SHPEH [1]

| Parameters | Units | Values |
|---|---|---|
| Diameter of the piezoelectric disk | mm | 25 |
| Diameter of a copper substrate | mm | 50 |
| Thickness of the piezoelectric disk | mm | 0.2 |
| Thickness of the copper substrate | mm | 0.2 |
| Density of PZT-5H | $kgm^{-3}$ | 7500 |
| Copper density | $kgm^{-3}$ | 8960 |
| PTFE density | $kgm^{-3}$ | 2200 |
| Young modulus of copper substrate | GPa | 110 |
| Young modulus of PTFE | GPa | 0.28 |
| Piezoelectric constant | $pCN^{-1}$ | 670 |

It also makes clear the dissipation of energy that occurs during the energy capture process using stacked piezoelectric disks. It has been shown that the main factor influencing voltage is the pulse's amplitude rather than the static pressure.

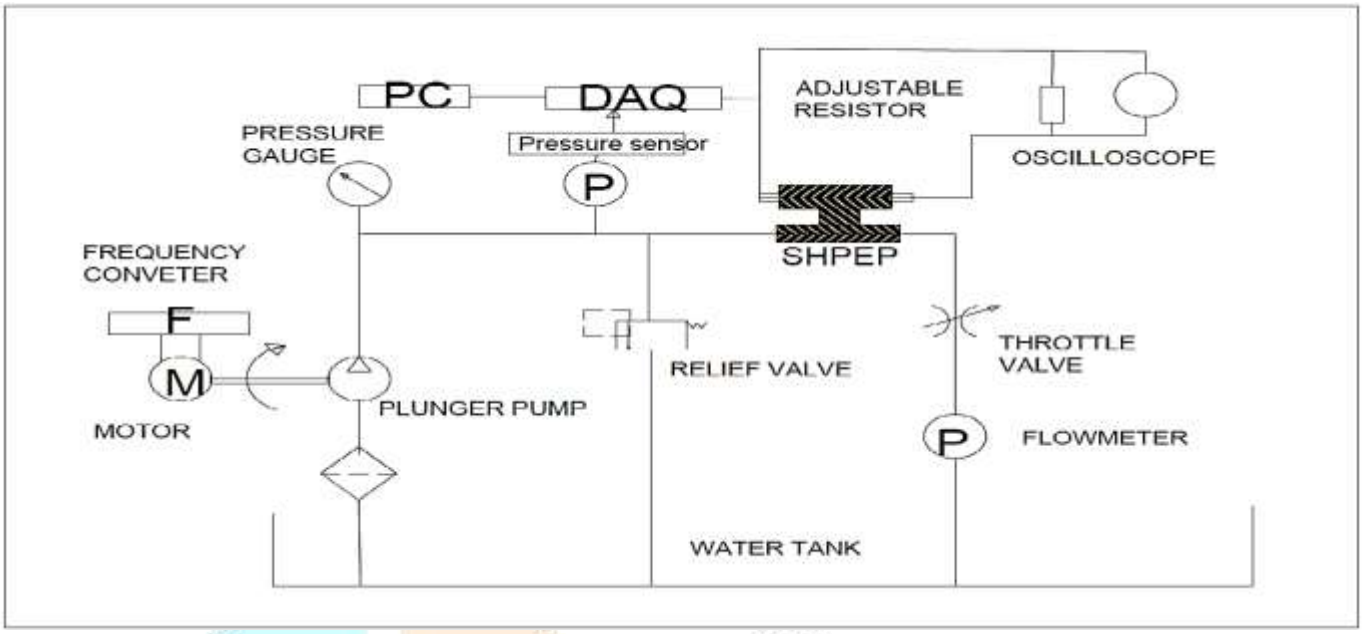


**Fig 1.** Experimental Symmetric Diagram [1]

The study also covers the consistency of power generation over multiple channels at once.

**Table 2** Performance parameters of the data acquisition system [1]

| Name | Model | Function | Measuring range | Measurement accuracy |
|---|---|---|---|---|
| Data acquisition cards | ADVANTECH (USB-4711A) | Signal acquisition | 10 MPa | 0.1% |
| Oscilloscope | RIGOL (DS1104Z) | Transient voltage acquisition | 100 MHz | 1 GSa $s^{-1}$ |
| Pressure sensors | MEACON (SUP-P300) | Transient pressure acquisition | -- | -- |
| Flow meter | – | Measure flow velocity | 1.2m3 h_1 | 1.0% |
| Adjustable resistance | Do More (ZX21f ) | Load resistors | 100MΩ | 0.5% |

It is examined whether there is a proportionate relationship between single-channel and multi-channel power generation.

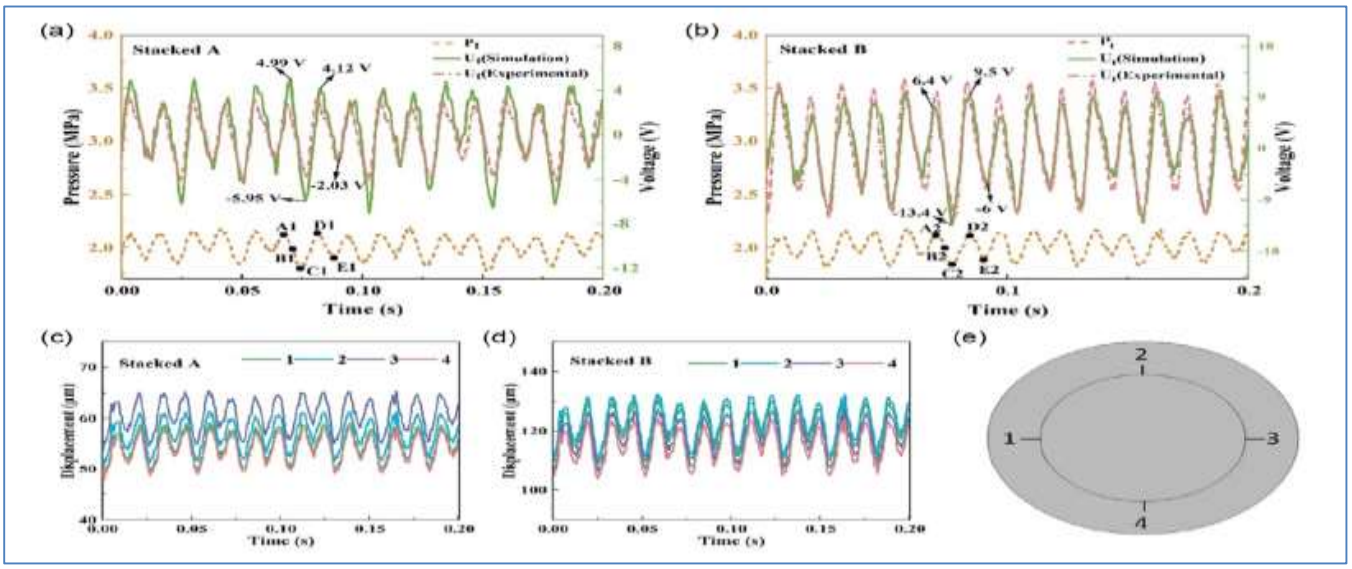


**Fig 2** a) Transient energy-harvesting characteristics. b) Pressure and voltage. d) The displacement of each point. e) The location of each point [1]

| **Table 3.** f) Tabulated deformation diagram of two piezoelectric disks [1] | | |
|---|---|---|
| **S.No** | **Deformation Location** | **Deformation in (µm)** |
| 1 | A1 – A2 | (0-20) , (100-160) |
| 2 | B1 – B2 | (0-40) , (120-160) |
| 3 | C1 – C2 | (0-45) , (125-160) |
| 4 | D1 – D2 | (0-50) , (130-160) |
| 5 | E1 – E2 | (0-60) , (135-160) |

Each connection's root mean square (RMS) voltage rises sharply with resistance [1]

| **Table 4** Comparison of PHEs [1] | | | | | | |
|---|---|---|---|---|---|---|
| **References** | **Piezoelectric material** | **Structure type** | **Pressure [MPa]** | **Frequency [Hz]** | **Power [µW]** | **Power density [µW(barmm3)$^{-1}$]** |
| This work [1] | PZT-5H (φ25 x 0.2mm$^3$) | Disk | 3 | 100 | 1155.63 | 1.774 |
| Shi et al. | PZT-5H (φ25 x 0.2mm$^3$) | Disk | 3 | 75 | 394 | 0.4 |
| Wang et al. | PZT-5H (φ25 x 0.2mm$^3$) | Disk | 0.4 | – | 9300 | – |
| Cao et al. | PZT-5H (5x5 x1mm$^3$x 9) | Stack | 3.5 | 100 | – | – |
| Aranda et al. | PZT Navy V(5x5 x9mm$^3$) | Stack | 22 | 100 | 33.5 | 0.149 |
| Cune fare et al. | PZT (6.8 x 6.8 x 30mm$^3$) | Stack | 3.5 | 450 | 1226 | 0.221 |
| Skow et al. | PZT-5A(6.8x6.8x 0mm$^3$) | Stack | 35 | 450 | 1000 | 0.721 |

### 2.2 High Power piezo pump for hydraulic actuation

Although control valves lose power, conventional valve-controlled hydraulic cylinders may not be as efficient.

| Table 5. PICA P025-50H ring stack parameters [2] | | | |
|---|---|---|---|
| **Parameter** | **Symbol** | **Valve** | **Unit** |
| Cross-sectional area | | 2.89 | $cm^2$ |
| Outer diameter | | 25 | Mm |
| Inner diameter | | 16 | Mm |
| Length | | 66 | Mm |
| Maximum voltage | | 1000 | V |
| Free displacement | x-max | 80 | Mm |
| Blocking force | F-block | 9.6 | kN |
| Capacitance | | 1.2 | mF |
| Natural Frequency | | 17 | kHz |

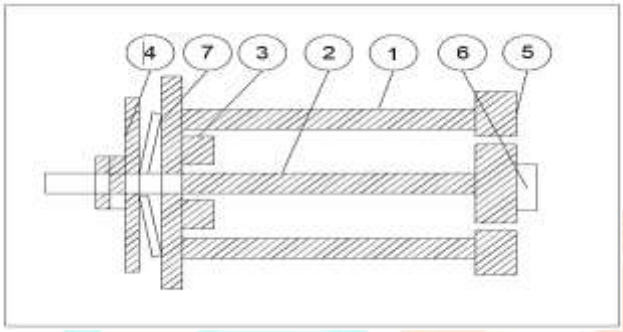


**Fig 3**. Cross-section of the piezo stack and piston assembly [2]

| S. No | Item | Material |
|---|---|---|
| 1 | Piezo stack | PIC151 |
| 2 | Piston Stainless Steel | 440C |
| 3 | Piston Clamp Stainless Steel | 440C |
| 4 | Belville washer spacer Copper | BS B32 |
| 5 | Inlet reed valve Stainless Steel | 440C |
| 6 | Valve screw Stainless Steel | 440C |
| 7 | Belville washer Carbon Steel | 51CrV4 |

Bill of Materials [2]

The electro-hydrostatic actuation system, along with servomotor-driven pumps, is an alternative. A piezo pump for sub-100 W aerospace applications, such as landing gear actuators, is presented in this study. With disc-style reed valves that permit pumping frequencies above 1 kHz, it has an output range of 10 to 100 W. Peak-to-peak sine wave stimulation at 950 V is provided via custom electronics.

| **Table 6**. Summary of Key Simulation Parameters [2] | | | |
|---|---|---|---|
| **Parameter** | **Symbol** | **Valve** | **Unit** |
| Bulk modulus | B | 0.8 | GPa |
| Density | rho | 850 | $kg/m^3$ |
| Young's modulus | E | 200 | GPa |
| Total stiffness | k-total | 120 | MN/m |
| Piezo damping | c-piezo | 5.6 | kNs/m |
| Chamber area | Ap | 560 | $Mm^2$ |
| Chamber length | L | 1 | Mm |
| Valve stiffness | k-spring | 1.16 | MN/m |
| Valve damping | c-free | 30.7 | Ns/m |
| Valve mass | m-valve | 0.53 | G |
| Discharge coefficient | Cd | 0.6 | |
| Valve diameter | d-valve | 16.5 | Mm |
| Valve thickness | t-valve | 200 | Um |

According to experimental results, there is no load on a hydraulic power up to 30W, and a flow rate of 2 L/min at 1250 Hz. Compact power electronics and high-frequency passive reed valves are examples of innovations.

For more electric aircraft, future research will concentrate on multi-cylinder pumps and enhanced reed-valve models [2].

### 2.3 Double-acting piezoelectric-hydraulic hybrid actuator

The issue of inertial force brought on by liquid flow pulsation typically plagues conventional single-acting piezoelectric-hydraulic hybrid actuators, reducing their output performance.

**Table 7. Specifications of packaged piezoelectric stack** [3]

| Parameters | Capacitance | Stiffness | Resonant frequency | Push/Pull force | Maximum/Nominal displacement |
|---|---|---|---|---|---|
| Values | 720 nF | 90 N/m | 23 kHz | 12000 N /1500 N | 105/80 µm |

To improve its output capabilities and reduce or eliminate the related inertial force, a novel double-acting piezoelectric-hydraulic hybrid actuator with four checks is proposed in this research—mechanical diode-like valves. The output performance of the newly constructed hybrid actuator was examined.

**Table 8. Comparison of the proposed hybrid actuator and other hybrid actuators** [3]

| Parameters | Sirohi and Chopra[13] | Mauck and Lynch[14] | Diao et al.[17] | Xuan et al.[32] | John et al.[33] | The proposed actuator |
|---|---|---|---|---|---|---|
| Voltage (Vp-p) | 100 | 800 | 500 | 1000 | 140 | 700 |
| Working frequency (Hz) | 300 | 60 | 600 | 250 | 600 | 450 |
| Maximum no-load velocity (mm/s) | 30.5 | 72.5 | 4.8 | 101 | 75 | 168.1 |
| Maximum blocking force (N) | 155.7 | 271 | 378 | 346 | 62.3 | 141 |

The pulsation rates, $\delta$ at 700 Vp-p and 2 MPa bias pressure are 2.29, 2.08, and 1.78 at 400 Hz, 500 Hz, and 600 Hz, respectively. For a single-acting hybrid actuator under identical circumstances, the pulsation rate is 10.98, 11.05, and 17.12 [3].

### 2.4 A Piezo-Electric Valve Actuator for Hydraulic Exoskeleton Drives

Due to its power density, hydraulic actuators are favoured in heavy lifting applications such as exoskeletons.

**Table 9**. Parameters for specification [4]

| **Quantitative Specifications** | | |
|---|---|---|
| **Description** | **Symbol** | **Valve** |
| Hydraulic Power | P | 800 W |
| System pressure | p | 200 bars |
| Actuation force | F | 10 N |
| Flow rate | q | 2,4 l/min |
| Switching time | t | <5 ms |
| **Qualitative Specifications** | | |
| Bistable endpoints (on/off) of the hydraulic valve | | |
| A small mass, e.g. 200 g | | |
| Small size, e.g. 50 mm x 30 mm x 20 mm | | |

With an emphasis on a piezo-actuator design that uses a bistable buckling beam to enhance the low strain of piezo materials, this research investigates the application of piezo-ceramics in electrically actuated hydraulic valves.

| **Table 10**. Parameters for buckling beam [4] | | |
|---|---|---|
| **Quantitative Specifications** | | |
| **Description** | **Symbol** | **Value** |
| Young's modulus | E | 210 GPa |
| Length | L | 26 mm |
| Width | B | 10 mm |
| Thickness | H | 0.3 mm |

Piezo stack integration, bearing design, and the snapping needs of the beam are major obstacles. The work describes a smooth drive and simulates the buckling beam, builds the actuator, and deals with bearing friction [4].

### 2.5 Flexural amplified piezoelectric actuators

Piezo-actuators can produce greater force and frequency of actuation. However, the actuator length can only be adjusted by 0.1%. These piezo-actuators can be used to create piezo-hydraulic pumps; however, higher actuation frequencies are required to obtain higher pump flow rates. This limits the application of these piezo pumps to higher-viscosity fluids at higher flow rates. As a result, various amplification procedures must be used to increase the displacement of piezo-actuators to preserve their maximum force-handling capacity.

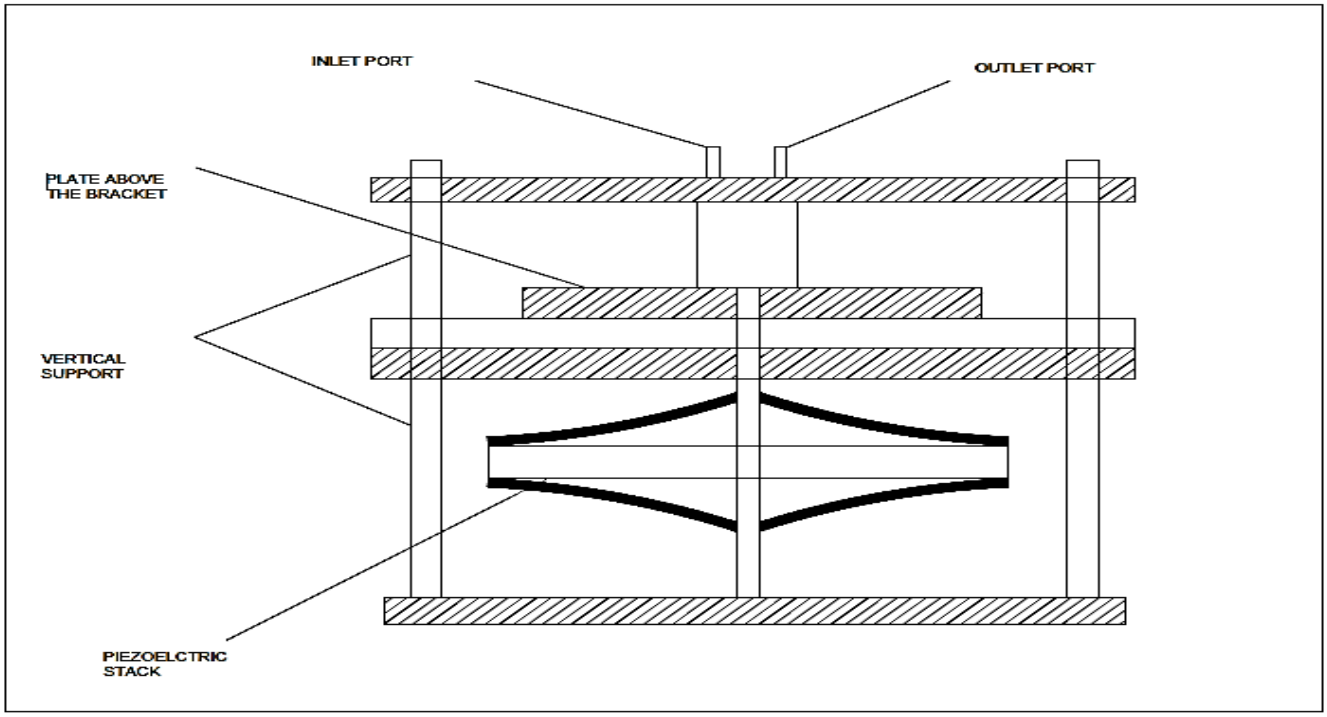


**Fig 4.** Sectional view of the design of the piezo-hydraulic pump [5]

There are numerous reports of piezo-hydraulic pumps that use flexurally amplified piezoelectric

| **Table 11.** Properties of MLA101020 piezoelectric stack actuator [5] | |
|---|---|
| **Model** | **MLA101020** |
| Displacement | 20 mm |
| Blocked Force | 4000 N |
| Stiffness | 200 N/mm |
| Resonant frequency (free-free) | 60000 Hz |
| Response Time | 0.008 ms |
| Voltage Range | -20 V–150 V |
| Capacitance | 4.4 mF |
| Resolution | 0.2 nm |
| Height | 20 mm |
| Length X Width | 10 mm x 16 mm |
| Mass | 15 |

actuators in the literature, although most of them are based on piezo actuators.

**Table 12.** Comparison of the flow rate measured using a flowmeter with the theoretical value [5]

| Frequency (Hz) | Experimental Pumping Displacement (mm) | Theoretical Flowrate (mL/min) | Flow rate using Measuring Cylinder (mL/min) | Flowrate using Flowmeter (mL/min) | %error between the flow meter and theoretical value |
|---|---|---|---|---|---|
| 1.0 | 369.0 | 25.550 | 25.2 | 25.36 | 0.75 |
| 2.0 | 366.0 | 49.810 | 50.4 | 49.10 | 1.45 |
| 3.0 | 360.0 | 73.490 | 72.4 | 70.95 | 3.58 |
| 4.0 | 350.0 | 95.264 | 93.6 | 92.80 | 2.66 |
| 5.0 | 340.5 | 115.850 | 114.0 | 113.10 | 2.43 |

Consequently, the objective of this work is to develop a piezo-hydraulic pump [5]

## 2.6 Piezoelectric micropumps

Three different types of piezoelectric micropumps with other configurations (single, series, and parallel connections) are designed and studied. The wet etching technology changes each micropump by sealing in high-temperature glass bonding.

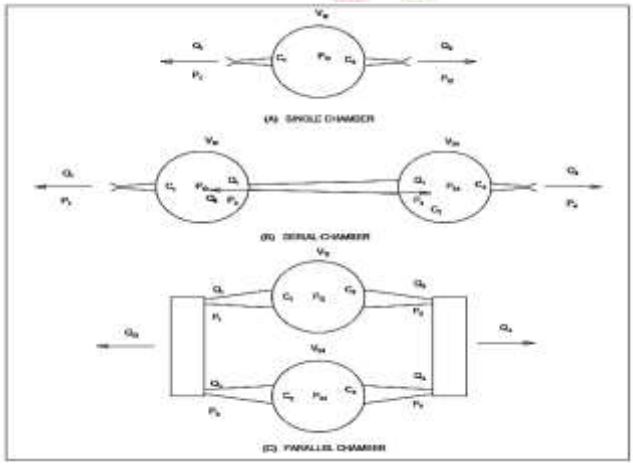

**Fig 5**. Schematic of micropump with (a) single, (b) series, and (c) parallel pump chambers [6]

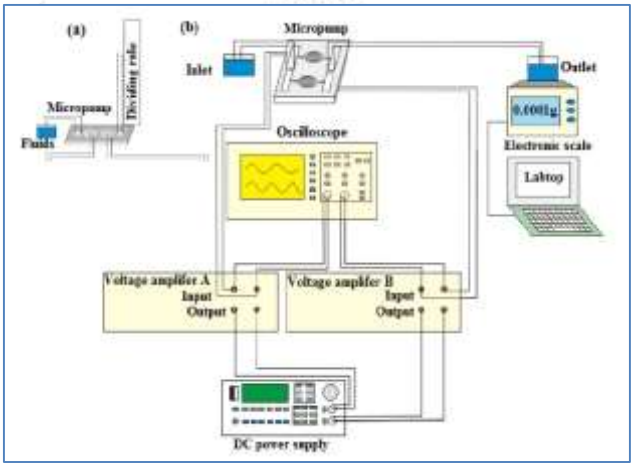


**Fig 6**. The schematic of the testing platform for measuring pressure head (a) and flow rate (b) [6]

They share the same microchannel dimension feature for the diffuser/nozzle. Verifying the impact of adding pump chambers in series or parallel on single chambers and confirming that the piezoelectric transducers' performance, three micropumps' pressure, and flow rate have all been examined. The micropumps with parallel-linked pump chambers have a higher flow rate than the micropumps with single and serially

connected pump chambers when the three types of micropumps are evaluated under the same driving conditions, over the pressure and flow rate of the serial micropump. The single, series, and parallel connection pump chambers for the micropumps have been designed and produced. The pressure and flow rates of three micropumps have been measured and analysed. The PZT transducer vibration displacement has been tested and examined to ascertain the reason for the differences in pressure and flow rate among the three types of micropumps [6].

**Table 13**. Parameters of the piezoelectric transducers [6],[8]

| Parameter | Value |
|---|---|
| Piezoelectric plate diameter | 11.3 mm |
| Piezoelectric plate thickness | 0.20 mm |
| Piezoelectric coefficient matrix ($C/m^2$) | $\begin{bmatrix} 0 & 0 & 0 & 0 & 17 & 0 \\ 0 & 0 & 0 & 17 & 0 & 0 \\ -6.5 & -6.5 & 23.3 & 0 & 0 & 0 \end{bmatrix}^T$ |
| Permittivity ε (F/m) | $\begin{bmatrix} 1.5 & 0 & 0 \\ 0 & 1.5 & 0 \\ 0 & 0 & 1.239 \end{bmatrix} \times 10^{-8}$ |
| Young's modulus (Pa) | $\begin{bmatrix} 1.7 & 0 & 0 \\ 0 & 1.7 & 0 \\ 0 & 0 & 1.58 \end{bmatrix} \times 10^{11}$ |
| Poisson's ratio | $\lambda_{12} = \lambda_{13} = \lambda_{23} = 0.3$ |
| Shear modulus (Pa) | $\begin{bmatrix} 0 & 2.33 & 2.3 \\ 0 & 0 & 2.3 \\ 0 & 0 & 0 \end{bmatrix} \times 10^{10}$ |
| Density ($kg/m^3$) | 1500 |
| Copper substrate diameter | 15 mm |
| Copper substrate thickness | 0.37 mm |
| Copper Young's modulus (Pa) | 0:9 $X10^{11}$ |
| Copper Poisson's ratio | 0.32 |
| Copper density ($kg/m^3$) | 8500 |
| Resonant frequency | 10.0 ±0.5 kHz |
| Impedance | 300 Ω |
| Capacitance | 9 nF±30% |

The pressure and flow rate shifting trends for single, series, and parallel micropumps are comparable. To be more precise, it climbs initially before declining as the frequency rises. Each curve had a maximum flow rate and a pressure value. Under identical driving conditions, the parallel micropump generates the highest flow rate and pressure of the three micropumps (200 Hz higher frequency), whereas the series micropump generates the lowest. The conceptual analysis and the experimental results are satisfactory. For both P1 and P2, the vibration displacement of the single and parallel micropumps was greater than that of the series micropump. The lone micropump's displacement fell between P1 and P2. These findings clarified the three types of micropumps, varying patterns in pressure and flow rate. These three types of micropumps have a wide range of uses combined. For instance, when electric fields cannot be applied in the microchannel, where fluid flow and pressure-based flow are especially desired, or when micro-injection is required in microfluidic systems. (The parameters of the piezoelectric transducer have been cited in the table) [6].

## 2.7 Piezoelectric hydraulic linear motor with self-monitoring

By introducing (PHLMVS), a piezoelectric hydraulic linear motor with velocity self-monitoring. The velocity and A3 sensing voltage have a strong association at a fixed frequency of 500 Hz. Additionally, the velocity and sensor voltage are fitted using the least-squares method. For PHLMVS with 0/ 50/ 100 g of loads, the correlation coefficient, R-2 is computed as 0.974, 0.982, and 0.978, in that order. It demonstrated a stronger association between the piezoelectric pump's flow rate and the A3 sensing voltage
[7].

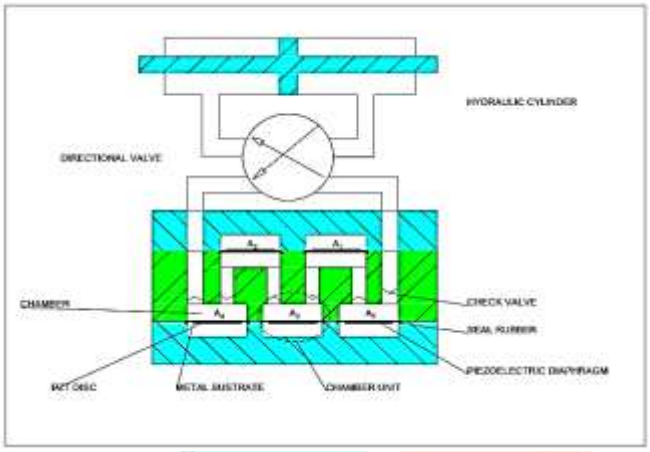


**Fig 7.** Semantic Diagram of PHLMVS [7]

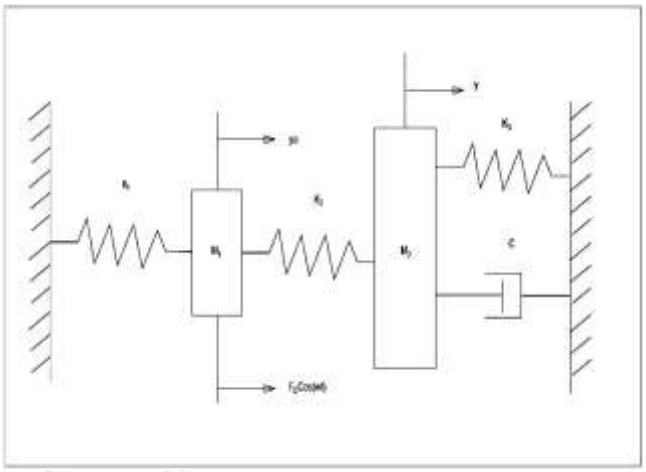

**Fig 8.** Dynamic model of PHLMVS [7]

Mathematical modelling was developed in this research paper for the theoretical analysis and experimental setup.

**Table 14.** Parameters of the piezoelectric hydraulic linear motor with velocity self-monitoring (PHLMVS) [7]

| S. No | Type | Numerical and materials |
|---|---|---|
| 1 | Pump size /mm | 150×60×22 |
| 2 | Pump material | PMMA |
| 3 | Check valve type | Umbrella valve |
| 4 | Check valve material | Silica gel |
| 5 | Diameter of metal substrate /mm | Ø41 |
| 6 | Thickness of metal substrate /mm | 0.4 |
| 7 | Metal substrate material | Brass |
| 8 | Diameter of PZT disc /mm | Ø25 |
| 9 | The thickness of PZT disc /mm | 0.2 |
| 10 | PZT disc material | Pb (ZrTi) O3 |
| 11 | Height of chamber /mm | 0.5 |
| 12 | Driving waveform | Sine wave |
| 13 | Hydraulic cylinder size /mm | 69.5x29x29 |

## 2.8 Micropump based on piezoelectrical transducer

Using finite element analysis, the parametric and vibrational properties of PZTs (Piezoelectric Transducers) with various diameters before and after coupling are examined. It is demonstrated that as the driving frequency increases, the piezo-electric transducer vibration stability decreases. According to vibration measurement, the PZT's maximum displacement variation with frequency exhibits the same pattern for various driving circumstances under both forced and free vibration (before and after sealing with the pump body). When forced to vibrate, the maximum displacement is lower than when allowed to vibrate freely. Under both free and induced vibration, the maximum displacement is exactly proportional to the driving voltage and inversely related to the transducer diameter. Different exterior diameters of diffuser/nozzle microvalves are used in the design and construction of micropumps.

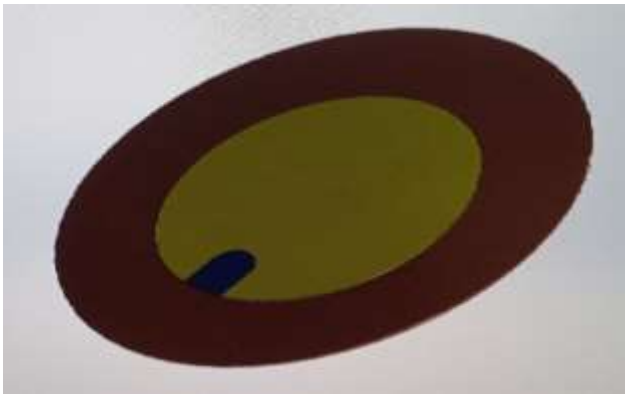

**Fig 9**. Structure of the piezoelectric transducer [8]

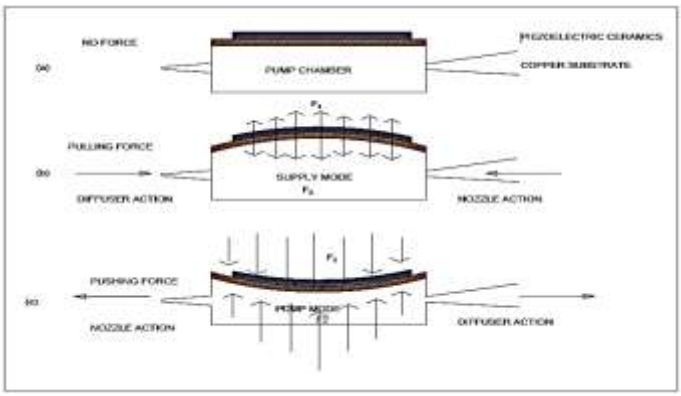


**Fig 10**. Working principle of the valveless micropump and the force diagram of the piezoelectric transducer. (a) No force. (b) Pushing force & supply mode. (c) Pulling force & pump mode [8]

Three types of micropumps with sandwich structures comprising these transducers were created utilising an enhanced DRIE process on a silicon wafer. Three piezoelectric transducers with exterior diameters of 12,15, and 20 mm were investigated and constructed for driving micropumps. The best driving parameters for the micropump and piezoelectric transducer were determined by the maximum vibrational displacement under forced and free vibration conditions, as well as before and after coupling. Ultimately, three micropumps were subjected to experimental measurements using various driving voltages, frequencies, and driving waves.

**Table 15**. Parameters of the piezoelectric transducers [8],[6]

| Parameter | Value |
|---|---|
| Piezoelectric plate diameter | 11.3 mm |
| Piezoelectric plate thickness | 0.20 mm |
| Piezoelectric coefficient matrix ($C/m^2$) | $\begin{bmatrix} 0 & 0 & 0 & 0 & 17 & 0 \\ 0 & 0 & 0 & 17 & 0 & 0 \\ -6.5 & -6.5 & 23.3 & 0 & 0 & 0 \end{bmatrix}^T$ |
| Permittivity ε (F/m) | $\begin{bmatrix} 1.7 & 0 & 0 \\ 0 & 1.7 & 0 \\ 0 & 0 & 1.58 \end{bmatrix} \times 10^{11}$ |
| Young's modulus (Pa) | $\begin{bmatrix} 1.7 & 0 & 0 \\ 0 & 1.7 & 0 \\ 0 & 0 & 1.58 \end{bmatrix} \times 10^{11}$ |
| Poisson's ratio | $\lambda_{12} = \lambda_{13} = \lambda_{23} = 0.3$ |
| Shear modulus (Pa) | $\begin{bmatrix} 0 & 2.33 & 2.3 \\ 0 & 0 & 2.3 \\ 0 & 0 & 0 \end{bmatrix} \times 10^{10}$ |
| Density ($kg/m^3$) | 7500 |
| Copper substrate diameter | 12, 15, 20 mm |
| Copper substrate thickness | 0.12, 0.37, 0.47 mm |
| Copper Young's modulus (Pa) | $0.9x10^{11}$ |
| Copper Poisson's ratio | 0.32 |
| Copper density ($kg/m^3$) | 8500 |
| Resonant frequency | 5.3±0.5 kHz, 10.0±0.5 kHz, 7.2_0.5 kHz |
| Impedance | 500, 300, 300 Ω |
| Capacitance | 15 nF±30%, 9 nF±30%, 12 nF±30% |

The following is a summary of the conclusions: Due to the liquid's counterforce, the piezoelectric transducer's average displacement following coupling with the pump body is lower than that before coupling. At low frequencies (i.e., below 1000 Hz), the PZT deforms in a nearly sinusoidal manner, and the vibration is constant. For each of the three piezoelectric transducers, the trend of variation with frequency of the maximum displacement of the nine measurement sites at the same driving voltage is the same for various driving waves. Due to the set boundary conditions in the former scenario, the maximum displacement under forced vibration is lower than that under free vibration. In comparison to other places, the piezoelectric transducer centre has a greater vibrational displacement. The greatest displacement is linearly proportional to the driving voltage and inversely proportional to the piezoelectric transducer diameters for both forced and free vibration situations. Under square wave driving, the displacement reaches its highest value; sine wave, triangle wave, and finally square wave follow. The PZT's ideal diameter is 12 mm. At a driving voltage of 100 Vpp and a square driving signal, the micropump performs efficiently. Under identical driving circumstances, the micropump's flow rate and pressure exhibit the same trends as the maximum displacement. Additionally, under the same driving circumstances, the patterns in the experiment's results match those in the vibrational measurement. Two values for the peak driving frequency exist at 60 hertz. (The parameters of the piezoelectric transducer values cited in the paper) [8]

### 2.9 Multiple piezoelectric pumps in a hybrid actuator

The piezoelectric hybrid actuator is a revolutionary electro-hydrostatic actuator with great potential for future development. The lightweight, compact, and low-power consumption of the piezoelectric hybrid actuator set it apart from the traditional hydraulic pump. However, its well-known drawback—that is, its low actuation force—keeps it from being used in real-world situations.

**Table 16**. Performances of piezoelectric hybrid actuator generalisation over the last 15 years [9]

| Developer | Mauck and Lynch (2000) | Sirohi and Chopra (2003) | Cadou and Zhang (2003) | Ellison (2005) | Tan et al. (2005) | Sirohi et al. (2005) | John et al. (2008) | Chaudhuri et al. (2009) | Chaudhuri and Wereley (2010) | Xuan et al. (2014) |
|---|---|---|---|---|---|---|---|---|---|---|
| Maximum force (N) | 271 | 155.7 | 49.9 | 62.23 | 225 | 71.1 | 31 | 92 | 63 | 346 |
| Maximum velocity (mm/s) | 72.5 | 30.5 | 15.7 | 228.6 | 39 | 139.7 | 50 | 98 | 330 | 101 |

To increase the greatest force produced by a single piezoelectric pump design, researchers have resorted to using several piezoelectric pumps due to limitations in the power supply and piezoelectric materials.

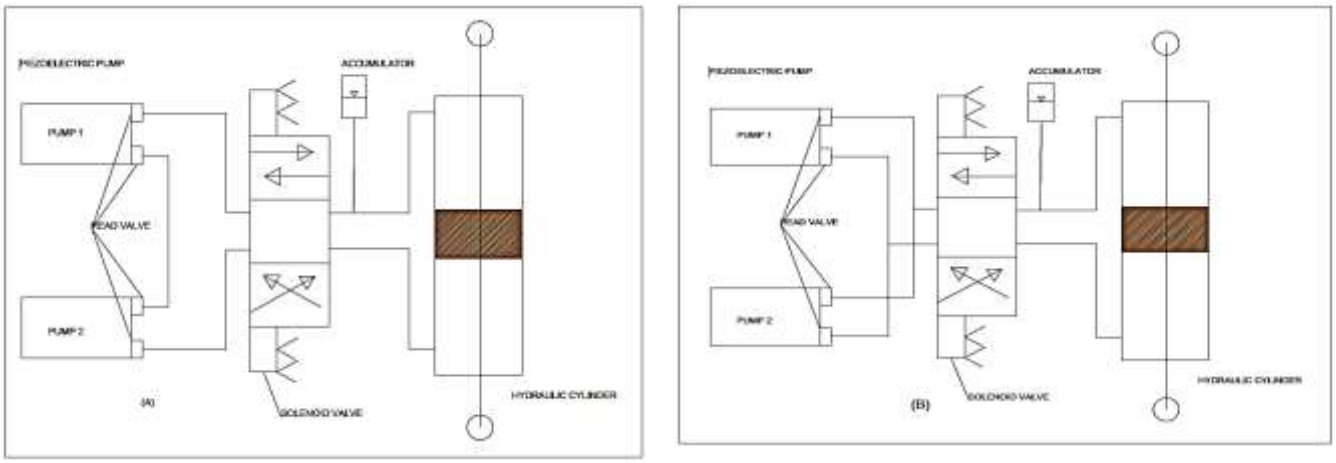


**Fig 11**. Connection method of a double-piezoelectric pump hybrid actuator: (a) series connection and (b) parallel connection [9]

In this study, a hybrid actuator including a hydraulic cylinder and a double-piezoelectric pump was designed, constructed, and tested to increase the actuation force.

**Table17**. Piezo-stack properties used in the double-piezoelectric pump hybrid actuator [9]

| Type | Size (mm) | Max. displacement (mm) | Stiffness (N/mm) | Blocking force (N) | Capacitance (nF) | Maximum driving voltage (V) | Resonant frequency (kHz) |
|---|---|---|---|---|---|---|---|
| P-025.40P | 60 (L) 3 25 (D) | 60 | 220 | 13,000 | 1300 | 1000 | 19 |
| Pst 1000/25/80 | 72×25(L x θ) | 105/80 | -- | 20000 | 1700 | 1000 | 15 |

Crucial design components, like driving and connecting techniques, were examined [9]

**Table 18**. Power amplifiers are used in the double-piezoelectric pump hybrid actuator [9]

| Type | Output voltage (V) | Peak current (mA) | Input impedance (kO) |
|---|---|---|---|
| E-481 | 0–1100 | 2000 | 100 |

Data were taken from the reference (PI Ceramic, 2012).

**Table 19**. Material properties of DTE-24 [9]

| Hydraulic fluid | Density ($kg/m^3$) | Kinematic viscosity (cSt) | Thermal conductivity (W/m K) | Specific heat capacity (J/kg K) | Molar mass (kg/kmol) |
|---|---|---|---|---|---|
| Mobil DTE-24 | 871 | 36 | 0.6069 | 4181.7 | 18.02 |

**Table 20**. Material properties of stainless steel [9]

| Solid | Density ($kg/m^3$) | Young's modulus (GPa) | Poisson's ratio | Bulk modulus (GPa) | Shear modulus (GPa) |
|---|---|---|---|---|---|
| Stainless steel | 8002.3 | 193 | 0.31 | 169 | 74 |

**Table 21**. The maximum blocking force and no-load velocity of the three designs [9]

| Three double-pump design | Maximum blocking force (N) | Maximum output velocity (mm/s) |
|---|---|---|
| CDSC-φ21-mm cylinder | 1841 | 68.3 |
| CDPC-φ30-mm cylinder | 2323 | 38.9 |
| CDSC-φ30-mm cylinder | 4615 | 29.4 |

CDSC: cross driving–series connection; CDPC: cross driving–parallel connection.

## 2.10 Hysteresis compensation using the Prandtl-Ishlinskii model

Researchers have long investigated the prospect of using piezoelectric ceramics or other smart materials to actuate proportionate flow control valves.

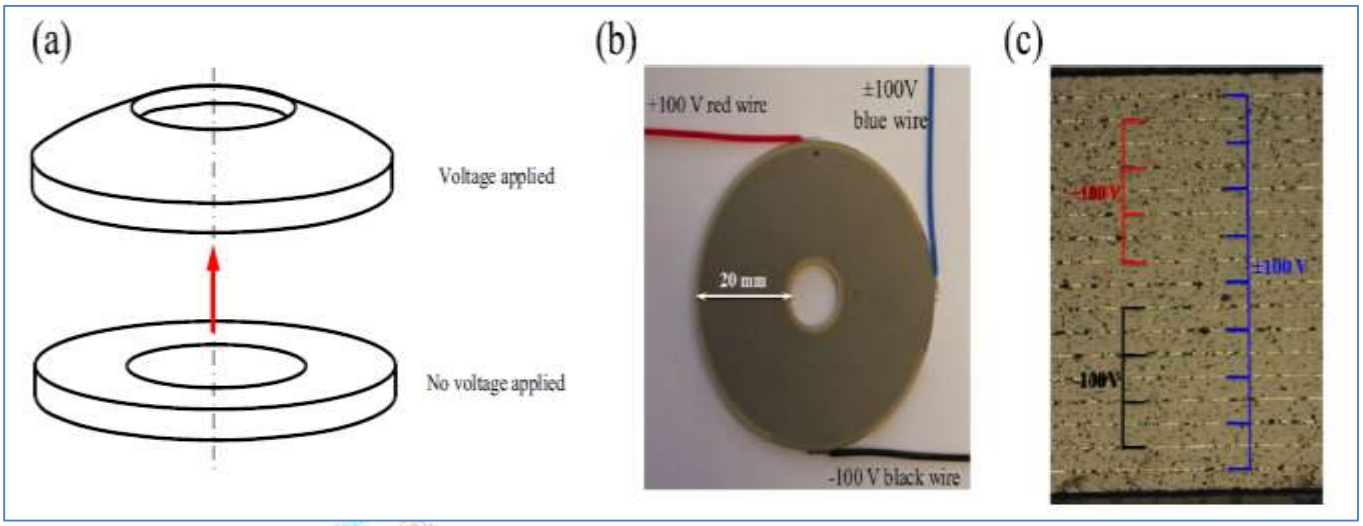


**Fig 12**. Piezoelectric ring bender deformation after application of electric field (a), multilayer piezoelectric ring bender (b), electrical connection, and (c) cross-section of Noliac CMBR08 actuator, the electrode spacing is 67μm for scale. (For interpretation of the references to colour in this fig., the reader is referred to the web version of this article.) [10]

Although performance increases over electromagnetic actuation have been demonstrated,

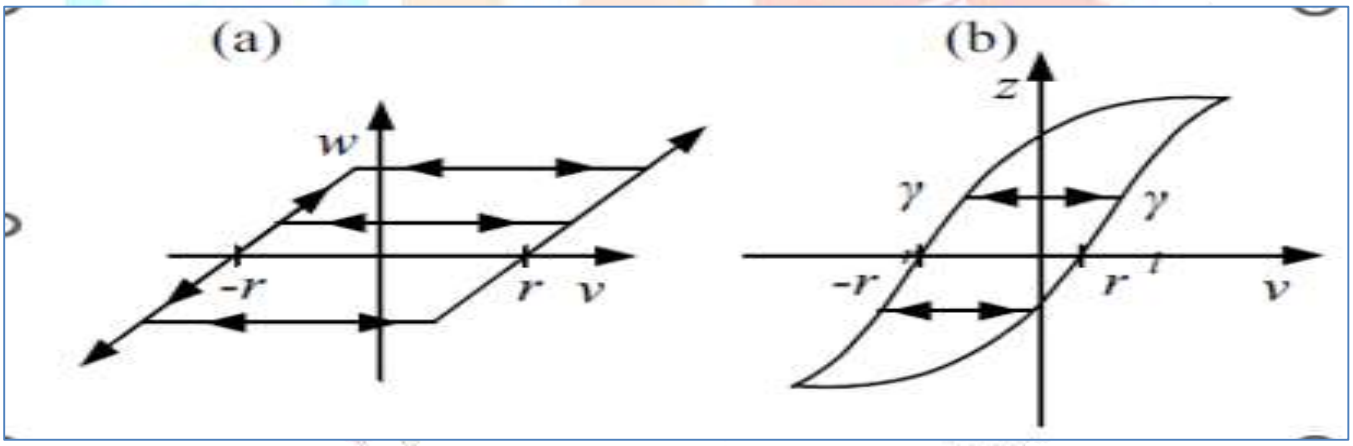


**Fig 13**. Classical play operator (a), generalised play operator (b) for Prandtl–Ishlinskii models [10]

Ferroelectric hysteresis (about 20% for a piezoelectric actuator) has proven to be a significant obstacle.

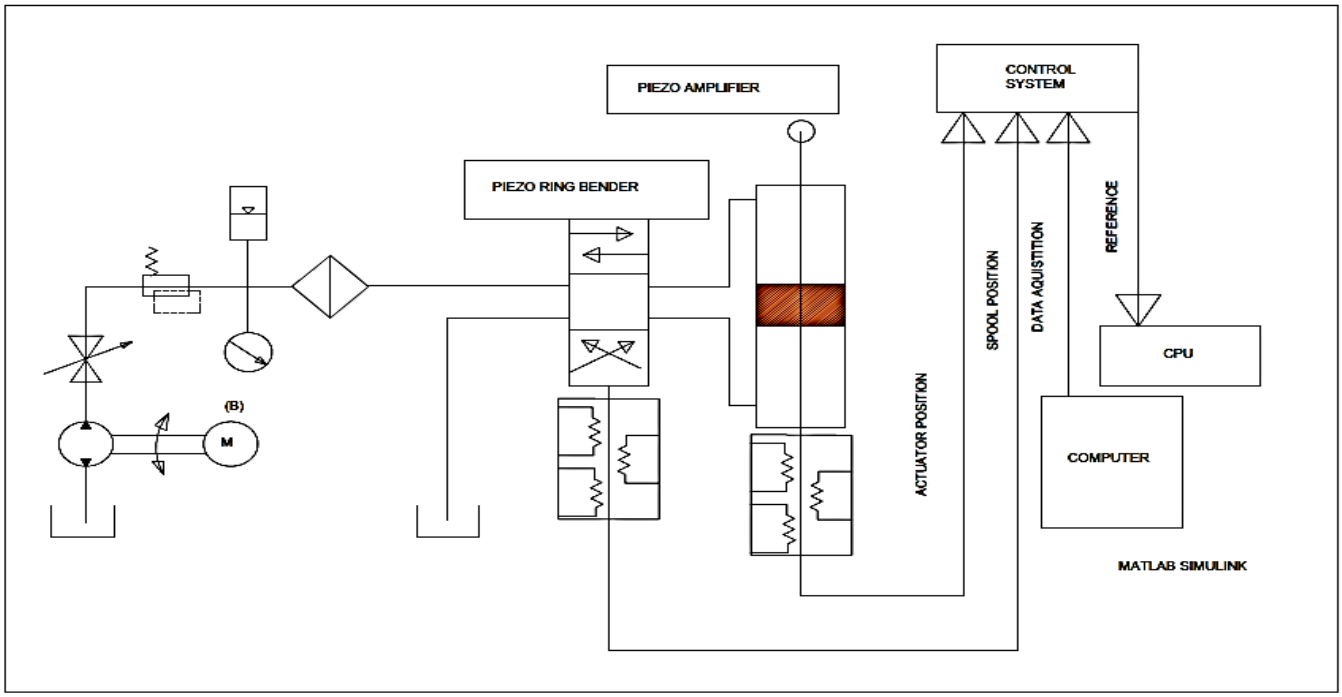


**Fig 14.** Semantic Diagram [10]

This study provides a comprehensive analysis of valve control methods, including hysteresis compensation for the first time. Experimental findings are obtained with a novel spool valve driven by a multi-layer piezoelectric ring bender. A generalised Prandtl-Ishlinskii model is fitted to experimental training data from the prototype valve to empirically model hysteresis.

**Table 22**. Frequency response results [10]

| Controller | Reference amplitude (mm) | OL | OL HC | PID | | | PID HC | | | FF PID G | | |
|---|---|---|---|---|---|---|---|---|---|---|---|---|
| | | | | 1 | 2 | 3 | 4 | 5 | 6 | 2 | 4 | 6 |
| -3dB frequency (Hz) | 35 | 25.1 | 39.6 | 96.1 | 164.6 | 77.6 | 119.5 | 124.9 | 118.7 | 102.5 | 102 | 109.9 |
| | 49 | 26.7 | 34.9 | 76.6 | 88.4 | 68.8 | 79.8 | 76.8 | 76.8 | 86.4 | 87.1 | 91.5 |
| -90° frequency (Hz) | 35 | 80.7 | 101.1 | 90.9 | 153.7 | 58.3 | 123.2 | 142.7 | 121.4 | 103.8 | 85.7 | 115.2 |
| | 49 | 83.9 | 104.9 | 107.1 | 142.8 | 62.4 | 137.7 | 145.1 | 135.5 | 90.7 | 68.5 | 90.4 |
| Resonant peak (dB) | 35 | 0 | 0 | 0.95 | 1.23 | 2.11 | 0.6 | 0.7 | 1.0 | 0.15 | 0.43 | 0.14 |
| | 49 | 0 | 0 | 0.8 | 0.7 | 1.2 | 0.43 | 0.45 | 0.58 | 0.16 | 0.23 | 0.15 |

**Table 23.** Results for different control Scenarios and PID constants [10].

| Controller | Acronym | $K_p$ | Ki | Settling time 5% (milliseconds) | | | | Overshoot (%) | | | |
|---|---|---|---|---|---|---|---|---|---|---|---|
| | | | | 17.5 | 52.5 | 87.5 | Avg | 17.5 | 52.5 | 87.5 | Avg |
| Reference amplitude (mm) | | | | | | | | | | | |
| PID Closed Loop Control | PID-1 | 1.1987 | 474.51 | 11 | 4.8 | 5.7 | 7.2 | 7.99 | 4.06 | 0.41 | 4.2 |
| | PID-2 | 2.3968 | 949.02 | 10.3 | 11.8 | 8.1 | 10.1 | 33.87 | 0.68 | 0.3 | 11.6 |
| | PID-3 | 0.5992 | 474.51 | 16.7 | 13.9 | 12.7 | 14.4 | 15.86 | 16.24 | 14.88 | 15.7 |
| | PID-4 | 1.1987 | 949.02 | 22 | 9 | 9.2 | 13.4 | 42.61 | 19.62 | 10.37 | 24.2 |
| | PID-5 | 1.1987 | 237.255 | 22.7 | 21.6 | 19.4 | 21.2 | 2.4 | 0.97 | 0.55 | 1.3 |
| | PID-6 | 0.5992 | 237.255 | 14.3 | 15.2 | 14.1 | 14.5 | 2.58 | 1.21 | 0.58 | 1.5 |
| PID with Hysteresis Compensation | PID HC-1 | 0.4823 | 190.916 | 14.2 | 17 | 17.1 | 16.1 | 2.05 | 0.97 | 0.58 | 1.2 |
| | PID HC-2 | 0.4823 | 213.898 | 11.4 | 15.1 | 14.5 | 13.7 | 2.75 | 1.21 | 0.69 | 1.5 |
| | PID HC-3 | 0.9645 | 427.796 | 12.2 | 9.8 | 6.5 | 9.5 | 4.67 | 0.97 | 0.58 | 2.2 |
| | PID HC-4 | 1.4468 | 641.595 | 10.6 | 7.6 | 7.2 | 8.5 | 6.94 | 1.09 | 0.69 | 2.9 |
| | PID HC-5 | 1.6879 | 748.544 | 4.1 | 7.2 | 7.4 | 6.2 | 1.92 | 3.44 | 3.67 | 3 |
| | PID HC-6 | 1.4468 | 748.544 | 4.4 | 11.7 | 7.4 | 7.8 | 7.17 | 5.59 | 4.34 | 5.7 |

This analytically invertible version of the model is used for both open-loop and closed-loop applications to correct for the hysteresis of the prototype valve [10]

## 2.11 Bidirectional hybrid piezoelectric hydraulic actuator

The hybrid piezoelectric-hydraulic actuator has a hydraulic pump driven by a piezo stack coupled to a conventional hydraulic cylinder.

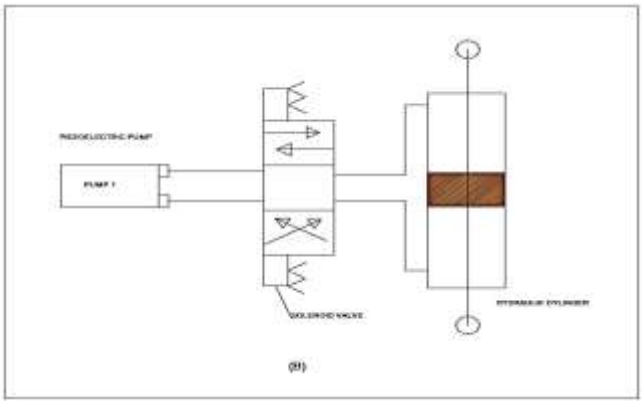

**Fig 15**. Configuration of the bidirectional hybrid actuator system [11]

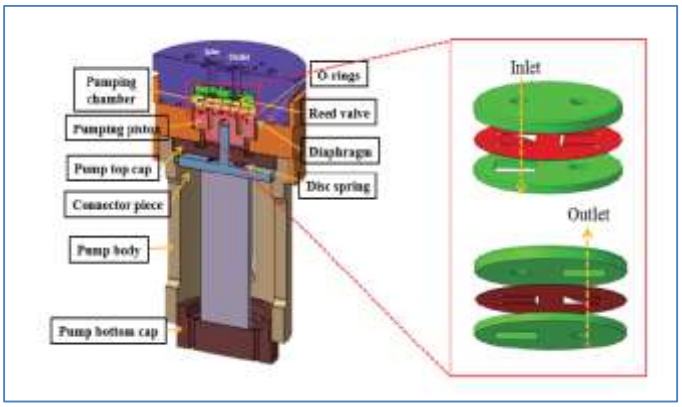


**Fig 16**. Section view of the pump assembly [11]

The actuator has a moderate energy output despite its compact size. Several developed nations are now investigating and creating these hybrid actuators due to the requirement for small and highly effective aircraft systems.

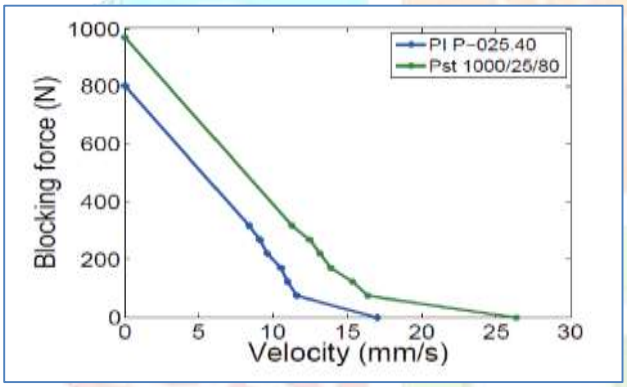


**Fig 17**. Force-velocity diagram of the two kinds of piezo stacks at 185Hz driving frequency, 2MPa bias pressure, and 0.05mm thickness of the reed valve [11]

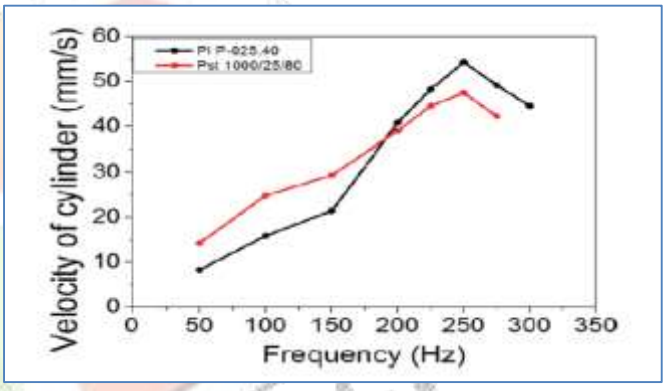


**Fig 18**. No-load velocity comparison of the two types of piezo-stacks at 1MPa bias pressure and 0.05mm thickness of the reed valve [11]

In a previous study, we designed and manufactured a unidirectional hybrid actuator. However, the blocking power was not as strong as expected. Thus, by removing the air bubbles and reworking the hydraulic cylinder and pump chamber, we improved the system in this study. Two different types of piezo stacks were used. Commercial solenoid valves were used to control the actuator's functioning in both directions. An actuator system with bidirectional functionality [11]

## 2.12 Design and Analysis of a Piezoelectric Hydraulic Pump

The ability of smart materials to deliver massive block forces in a small container while operating at high frequencies makes them particularly attractive for converting electrical power into mechanical power

**Table 24**. Pump geometry [12]

| Parameter | Symbol | Value (mm) |
|---|---|---|
| Pumping chamber diameter | dp | 31.75 |
| Discharge tube diameter | do | 1.5875 |
| Pumping chamber height | h | 0.254 |
| Discharge tube offset | R | 8.89 |
| Discharge tube length | l | 15.75 |

This has led to the development of hybrid actuators, which combine smart material-actuated pumps with hydraulic cylinders.

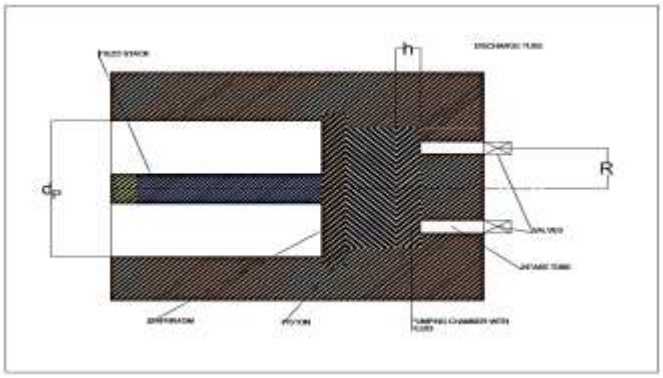


**Fig 19**. Schematic diagram of the pump illustrating the important design parameters like the pumping chamber height (h), the discharge tube location (R), the pumping chamber diameter (dp), and the discharge tube diameter (do) [12]

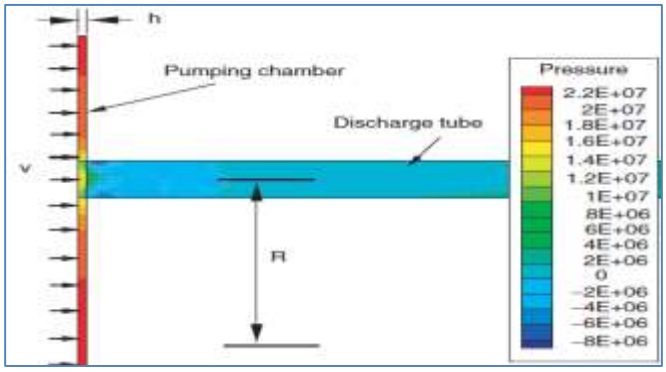


**Fig 20**. Computational domain for the 2D problem illustrating the boundary conditions and a sample pressure distribution [12]

The total success of the hybrid concept depends on how well the fluid and smart materials are coupled.

**Table 25**. Fluid properties [12]

| Parameter | Symbol | Value |
|---|---|---|
| Density | ρ | 850 kg/m$^3$ |
| Kinematic viscosity | ν | 3.61x10$^{-5}$m$^2$/s |

This research presents the results of two- and three-dimensional (2D and 3D) fluid flow simulations in a prototype hybrid actuator being developed for aeronautical applications

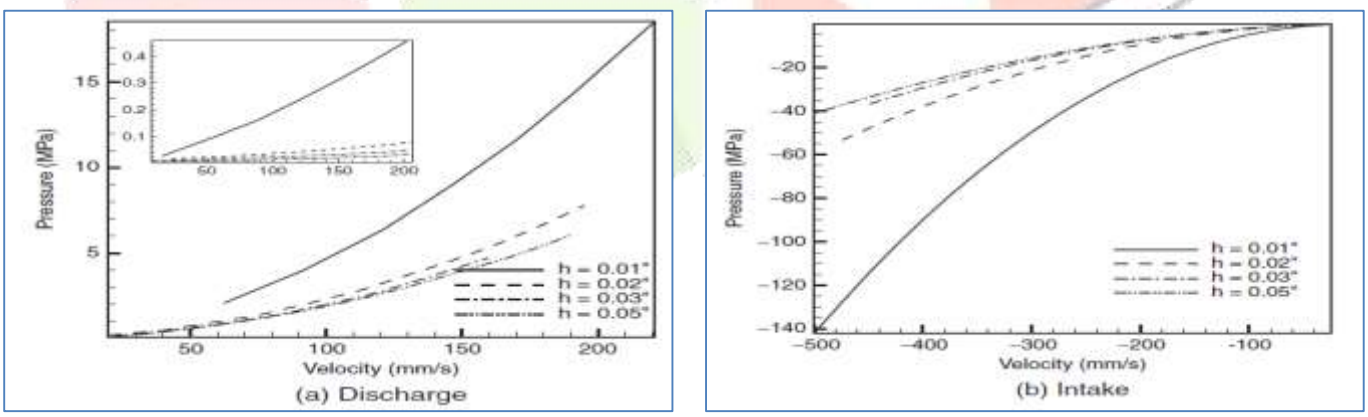


**Fig 21**. Pressure loss as a function of piston velocity for various pumping chamber heights, h. The inset in Figure (a) shows results from 2D simulations [12]

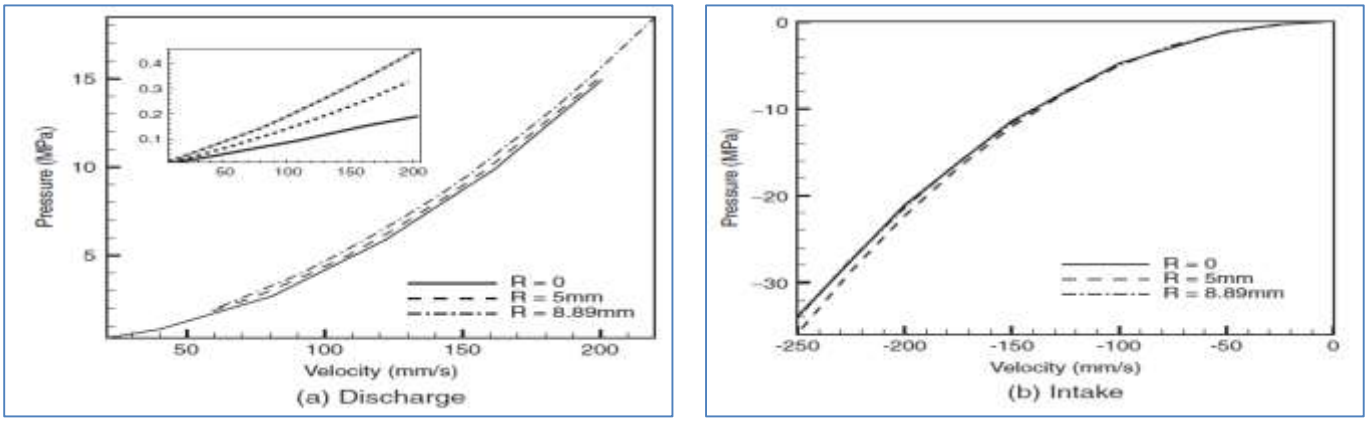


**Fig 22**. Pressure loss as a function of piston velocity for various discharge tube locations R. The inset in Figure (a) shows results from 2D simulations [12]

According to the simulations, the device loses the three-dimensional processes, which are the fluid's radial acceleration in the pumping chamber and the formation of vortex ring structures. In this section, the predictions from the updated analytical models for both intake and discharge processes are compared with the results of computational fluid dynamics (CFD). According to research by Aboubakri and associates, the previously mentioned analytical model defines pressure as a function of P-block, which is computed by dividing the piston area by the blocking force applied by the piezoelectric stack. Here, the loss coefficients associated with intake and discharge are denoted by k_dis and k_in, respectively. Aboubakri et al made clear that these coefficients represent the pressure losses within the system. For both the intake and discharge processes, a satisfactory alignment with the outcomes from computational fluid dynamics is obtained by choosing values of k_dis = 0.001 and k_in = 0.0005. The findings reveal a reasonable correlation for both discharge and intake operations. Notably, the application of a logarithmic scale accentuates the observable discrepancies between intake and discharge at lower frequencies, while reducing them at higher frequencies. Furthermore, the figure illustrates that the relative importance of pressure losses during discharge, in contrast to intake, fluctuates with the operating frequency. At frequencies below 100 Hz, the pressure losses associated with both discharge and intake are nearly indistinguishable to the piezo-stack. However, at frequencies exceeding 100 Hz, the pressure losses associated with intake are greater than those during discharge, rendering the force coupling with the piezo-stack more critical during the intake phase compared to discharge. This occurrence, along with the effects of cavitation, which are not accounted for in this simulation, may explain the abrupt decline in mass flow that has been experimentally observed at frequencies above 400 Hz (Simulation Analysis and Performance Test of a Compressible Piezoelectric Pump Fluid Cavity, 2023). Finally, the authors substantiate the initial hypothesis that the flow within the pump is both laminar and incompressible. Display of Reynolds number contours based on the height of the pumping chamber at the maximum flow rate examined in this study ($1.6x10^{-4}$ $m^3$ /s) for a conventional pumping chamber configuration. The picture demonstrates that the flow remains laminar (Re<2400) throughout, thereby confirming the appropriateness of omitting a turbulence model in the simulations. Similarly, the Mach number remains below 0.3 (Mmax = 0.17) within the flow field, indicating that the assumption of incompressible flow is valid for this investigation. Nevertheless, the actual impact of compressibility on this device is more complex than it suggests. The current research has shown that pressure differentials related to high-frequency pumping are considerable (59 MPa). Consequently, unless the system experiences an adequately high pre-load pressure (which is not practical for a functioning device), the effects of compressibility arising from two-phase flow conditions (i.e., cavitation) are likely to be substantial in a 'real' device. Conversely, the model implies correlating flow rate with operating frequency in this study likely overestimates the flow rate, as it does not consider the reduction in piezo stroke due to force feedback between the stack and the fluid. Therefore, to accurately evaluate the true impact of compressibility in these devices and to provide realistic performance predictions concerning frequency, it is imperative to resolve the fully-coupled unsteady problem, wherein the fluid within the pumping chamber is actuated by a piezo-stack while incorporating the force feedback between the fluid and the piezo-stack [12].

### 2.13 Dynamic Characteristics of a Piezo Hydraulic Actuator

Operating a piezoelectric hydraulic actuator at greater pumping frequencies can increase its power density; however, optimal design requires a thorough understanding of the device's dynamics.

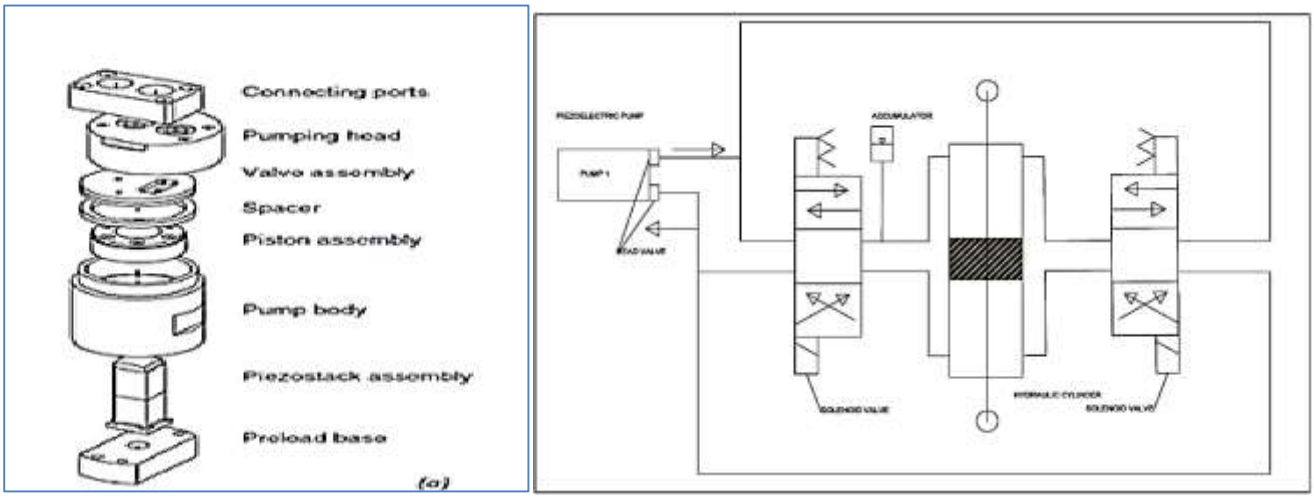


**Fig 23**. Piezo-hydraulic hybrid actuator: (a) Exploded view of the piezoelectric pump (b) schematic of the device [13]

This article explains how to use transmission line theory to build a frequency-domain model for the dynamic behaviour of a piezo-hydraulic actuator.

| **Table 26**. Prototype device parameters [13] | |
|---|---|
| **Piezo Stack – Model P-804.10** | |
| Number of piezo stacks | 2 |
| Length | 0.3937 in. |
| Width | 0.3937 in. |
| Height | 0.7087 in. |
| Blocking force (0-100 V) | 1133 lb |
| Free Displacement (0-100 V) | ~0.5 mil |
| Maximum voltage | 120 V |
| Minimum voltage | -24 V |
| Capacitance | ~7μF |
| **Hydraulic fluid – MIL-H-5606F** | |
| Density | 859 g/cc |
| Kinematic viscosity | 15 cSt |
| Reference bulk modulus $\beta_{ref}$ | 260,000 psi |
| **Pumping chamber** | |
| Diameter | 1 in. |
| Height | 0.050 in. |
| **Output actuator – double rod** | |
| Bore diameter | 0.4375 in. |
| Shaft diameter | 0.1875 in. |
| Stroke | 2 in. |

The investigation was done to look into how fluid viscosity and tube length affected the device's performance.

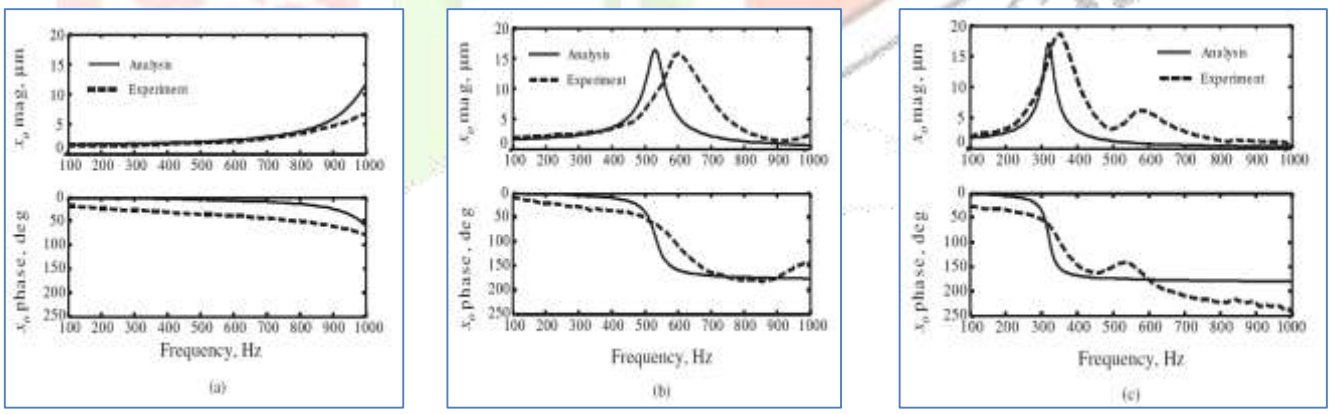


**Fig 24**. Comparison of experimental and analytical frequency response functions: (a) no tubes, pump directly attached to manifold; (b) tubing length=4.5 in.; and (c) tubing length=11.5 in [13]

As the length of the tube increases, the system's resonance frequency decreases. Similar to viscous damping, fluid viscosity has an impact on the system.

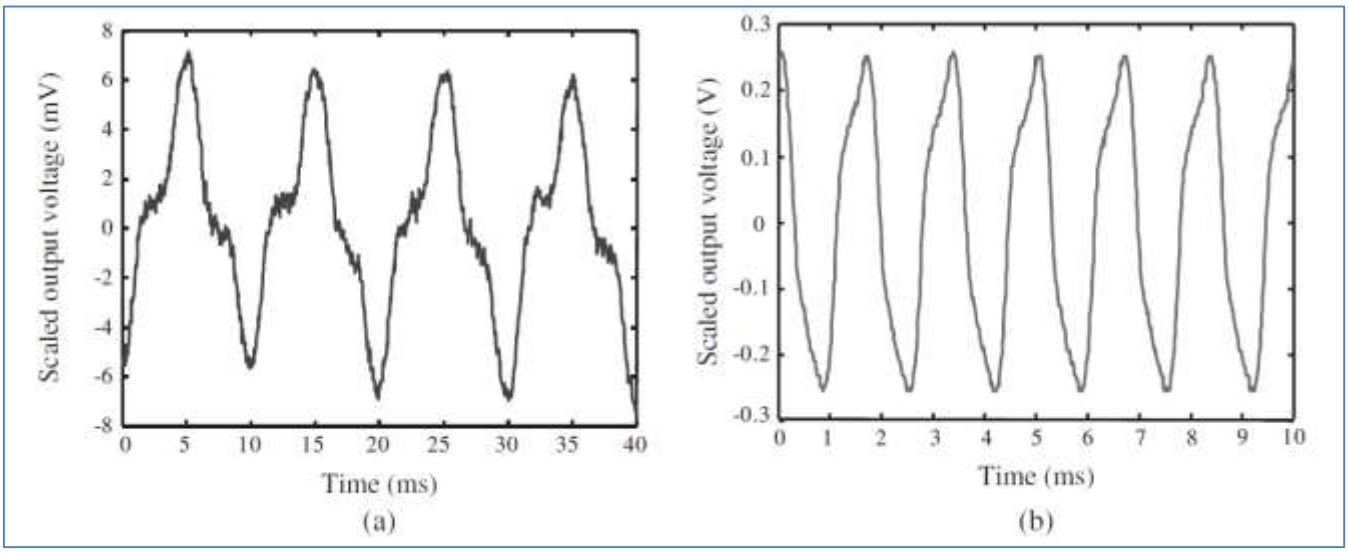


**Fig 25**. Vibrometer output signal in the time domain, actuation voltage amplitude 25 V: (a) pumping frequency 100 Hz and (b) pumping frequency 600 Hz [13]

Experiments conducted on a prototype piezo-hydraulic actuator validated the analysis.

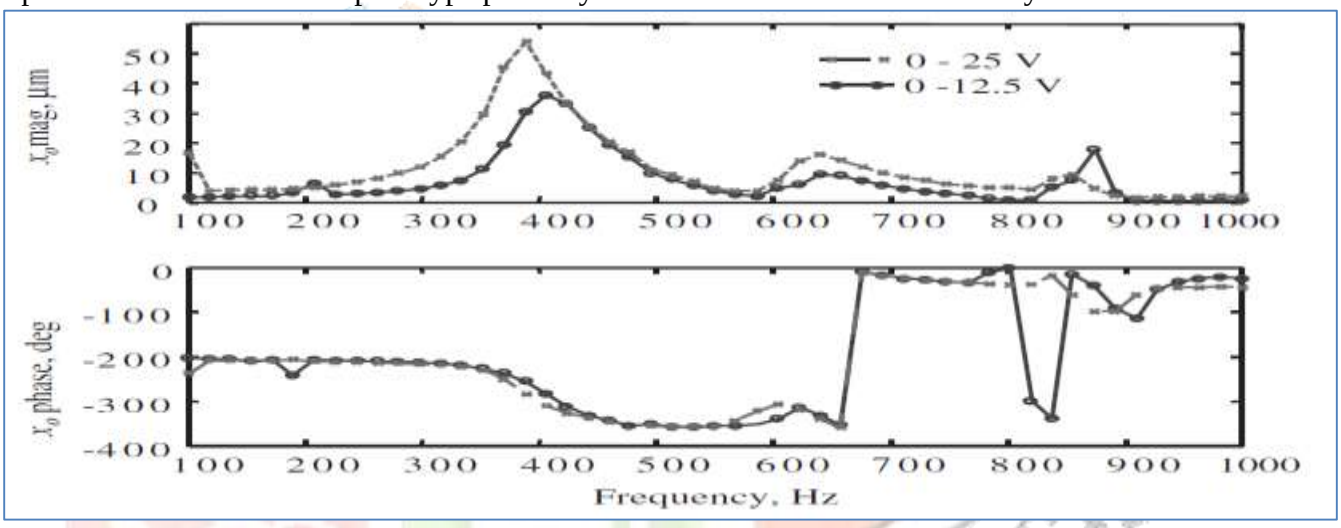


**Fig 26**. Effect of actuation voltage on the frequency response function [13]

The check valves on the flow rectification system were removed [13]

### 2.14 High Pumping Frequency Piezoelectric–Hydraulic Hybrid Actuator

The design and development of a piezoelectric–hydraulic hybrid actuator that operates at a high pumping frequency.

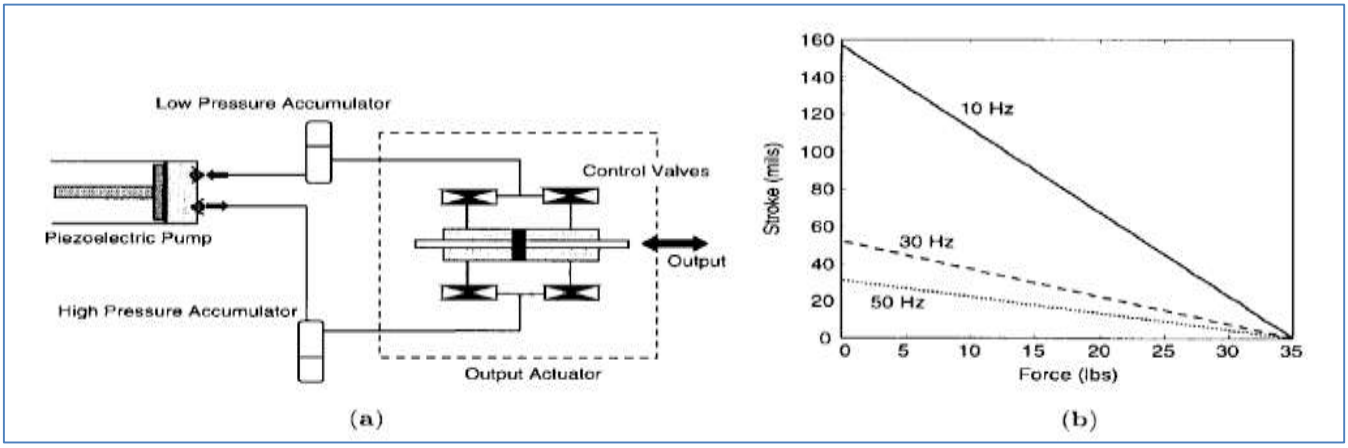


**Fig 27**. Piezoelectric-hydraulic hybrid actuator: (a) Schematic; (b) Normal output design goals [14]

The actuator is envisioned as a potential trailing-edge flap actuator for a full-scale smart rotor system. While earlier studies based on the same concept have examined actuators with huge piezoelectric stacks working at a relatively low pumping frequency, the current study aims to investigate the actuator's behaviour at a low volumetric displacement and high pumping frequency.

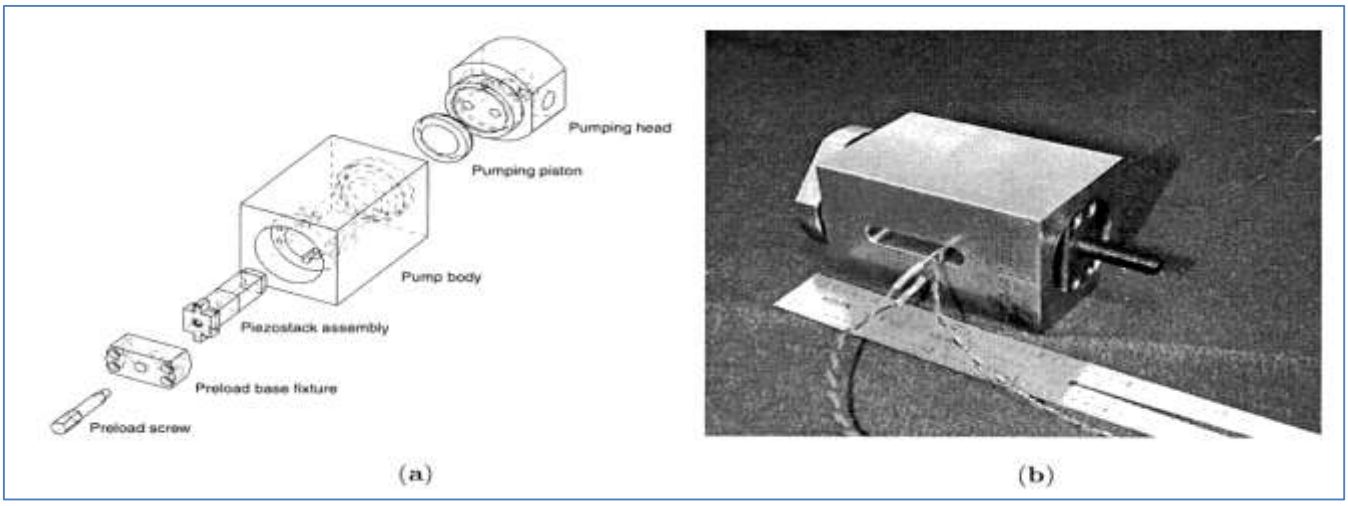


**Fig 28**. Prototype piezoelectric-hydraulic pump: (a) Exploded view; (b) First assembled prototype [14]

The first design of the actuator system is finished, and the effects of various system parameters on the actuator's operation are ascertained.

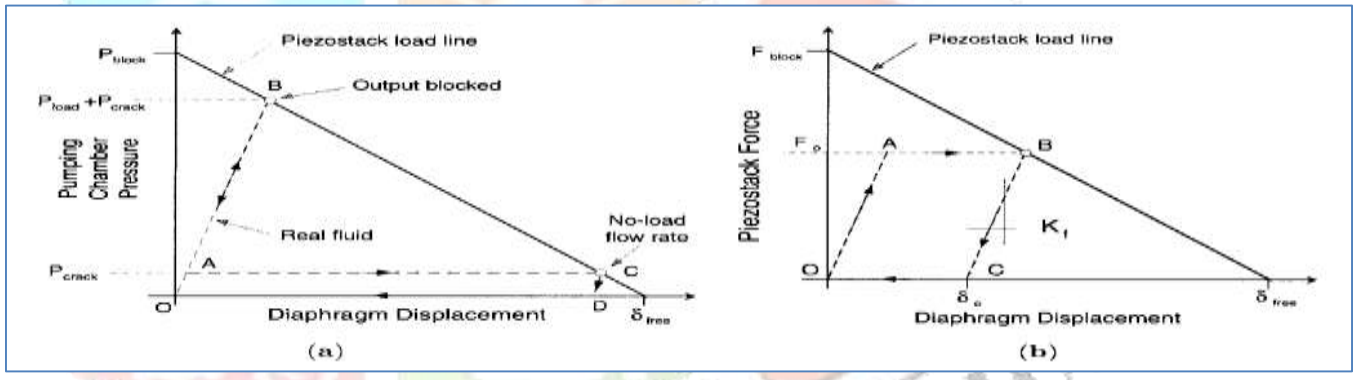


**Fig 29**. Typical pumping cycles for a real working fluid: (a) Limits of operation; (b) Load-line analysis [14]

This enables the selection of the ideal piezo-stack characteristics and geometric parameters for a given external load [14].

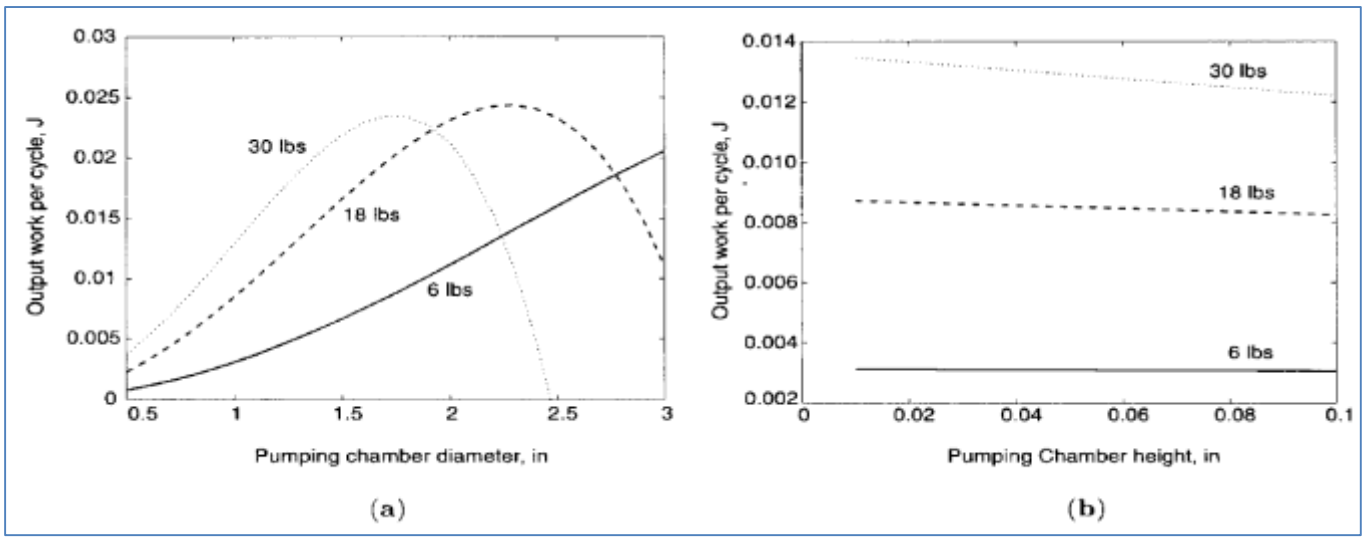


**Fig 30**. Dependence of work output per cycle on pumping chamber geometry: (a) Work output as a function of pumping chamber diameter, $\Delta_{gap}$ = 0:0500; (b) Work output as a function of pumping chamber height, $d_{cham}$ = 100 [14]

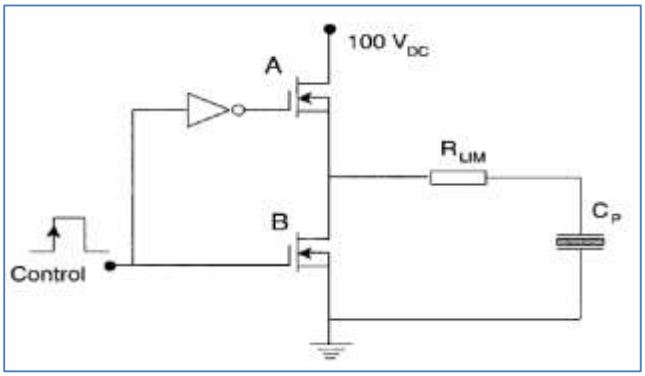


**Fig 31**. Schematic of the piezo-stack switch driver circuit [14]

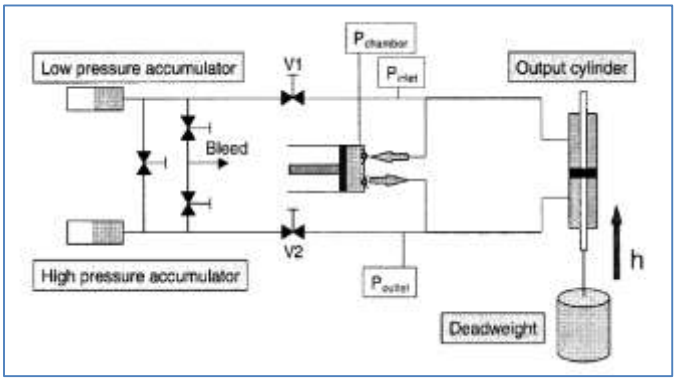


**Fig 32**. Experimental setup for the evaluation of unidirectional actuator performance [14]

A thorough analytical model of the device, which takes into account valve dynamics, hydraulic-circuit dynamics, and fluid inertia, must be created and verified to gain a better understanding of the dynamics of the hydraulic tubing and fluid, and potentially these effects, to increase the device's output flow rate. Only by raising the pump's flow rate can the output stroke and bandwidth be increased.

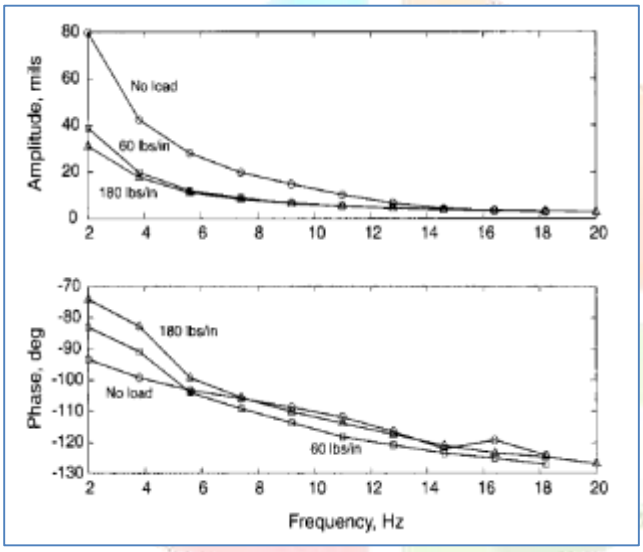


**Fig 33**. Output cylinder stroke as a function of output frequency, with external spring load, at 300 Hz pumping frequency [14]

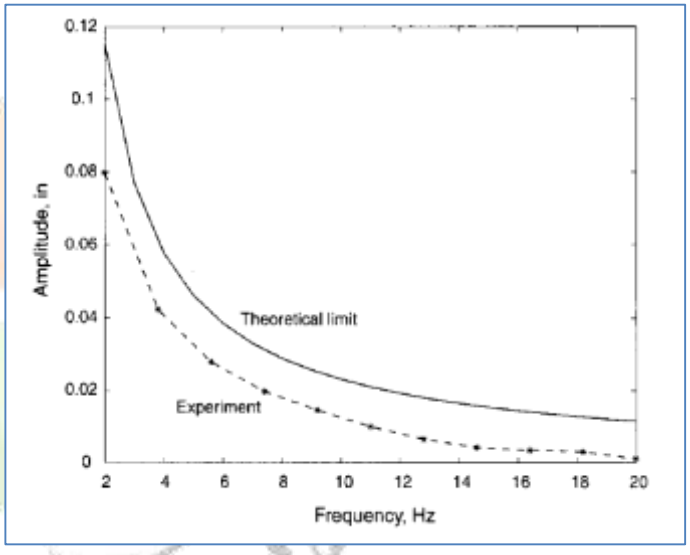


**Fig 34**. Correlation of measured no-load output displacement with predicted value at 300 Hz pumping frequency [14]

## III. CONCLUSION

This article is useful for researchers to utilizes data collections in their research work. Recent research journals have now developed a simple quasi-static model to improve the performance of fluid systems in piezo-hydraulic actuators. The Physik Instrumente (PI) LP, which manufactures vital equipment for numerous purposes, is headquartered at 16 Albert Street, Auburn, MA 01501. Significant progress in material development, energy harvesting application optimizations, and integration with new technologies are the future developments in piezoelectric technology. These advancements are growth for industries like structural health monitoring and wearable technologies. According to a recent study, pulse amplitude, non-static pressure, is the primary element affecting voltage. Because control valves lose power, traditional valve-controlled hydraulic cylinders may not be as efficient. Servomotor-powered independent pumps with electro-hydrostatic actuation are future research work directions.

## IV. DECLARATION OF COMPETING INTEREST

The author declares that there are no known competing financial interests or personal relationships that could have appeared to influence the work reported in this paper.

## V. REFERENCES

[1] W. Zhang, Y. Shang, H. Jiang, F. Meng, H. Zhao, and W. Shi, "Simulation and Experimental Research on a New Symmetrical Hydraulic Piezoelectric Energy Harvester," Energy Technol., vol. 12, no. 11, pp. 1–14, Nov. 2024, doi: 10.1002/ente.202400867.

[2] N. Sell et al., "Design and testing of a high power piezo pump for hydraulic actuation," J. Intell. Mater. Syst. Struct., vol.35, no. 14, pp. 1166–1177, Aug. 2024, doi: 10.1177/1045389X241256830.

[3] J. ZHANG and Z. FENG, "Design and identification of a double-acting piezoelectric-hydraulic hybrid actuator," ChineseJ. Aeronaut., vol. 37, no. 3, pp. 456–467, 2024, doi: 10.1016/j.cja.2023.06.024.

[4] P. Albrecht-Zagar and R. Scheidl, "A Piezo-Electric Valve Actuator for Hydraulic Exoskeleton Drives," Int. J. Fluid Power, vol. 23, no. 3, pp. 453–468, Sep. 2022, doi: 10.13052/ijfp1439-9776.23310.

[5] S. Nayak and M. Rao, "Design and development of a flexurally amplified piezoelectric actuator based piezo-hydraulic pump," Mater. Today Proc., vol. 46, no. xxxx, pp. 9956–9965, 2021, doi: 10.1016/j.matpr.2021.03.314.

[6] Y. Guan, M. Bai, X. Meng, Y. Liu, and F. Xu, "Experimental Investigation of Piezoelectric Micropumps with Single, Series or Parallel Pump Chambers," Int. J. Acoust. Vib., vol. 25, no. 3, pp. 453–460, Sep. 2020, doi: 10.20855/ijav.2020.25.31688.

[7] C. Qian, S. Chen, J. Wang, J. Kan, Z. Zhang, and M. Yu, "A piezoelectric hydraulic linear motor with velocity self-monitoring," Sensors Actuators A Phys., vol. 306, p. 111962, May 2020, doi: 10.1016/j.sna.2020.111962.

[8] Y. Guan, X. Meng, Y. Liu, M. Bai, and F. Xu, "Modeling, Vibration Analysis and Fabrication of Micropumps Based on Piezoelectric Transducers," Int. J. Acoust. Vib., vol. 25, no. 3, pp. 383–391, Sep. 2020, doi: 10.20855/ijav.2020.25.31670.

[9] Y. Li, V. T. Le, N. S. Goo, T. H. Kim, and C. S. Lee, "High actuation force of piezoelectric hybrid actuator with multiple piezoelectric pump design," J. Intell. Mater. Syst. Struct., vol. 28, no. 18, pp. 2557–2571, Nov. 2017, doi: 10.1177/1045389X17692048.

[10] F. Stefanski, B. Minorowicz, J. Persson, A. Plummer, and C. Bowen, "Non-linear control of a hydraulic piezo-valve usinga generalised Prandtl–Ishlinskii hysteresis model," Mech. Syst. Signal Process., vol. 82, pp. 412–431, Jan. 2017, doi: 10.1016/j.ymssp.2016.05.032.

[11] X. L. Jin et al., "Experimental Study on the Performance of a Bidirectional Hybrid Piezoelectric-Hydraulic Actuator," Int. J. Aeronaut. Sp. Sci., vol. 16, no. 4, pp. 520–528, Dec. 2015, doi: 10.5139/IJASS.2015.16.4.520.

[12] S. John, C. Cadou, J.-H. Yoo, and N. M. Wereley, "Application of CFD in the Design and Analysis of a Piezoelectric Hydraulic Pump," J. Intell. Mater. Syst. Struct., vol. 17, no. 11, pp. 967–979, Nov. 2006, doi: 10.1177/1045389X06062142.

[13] J. Sirohi, C. Cadou, and I. Chopra, "Investigation of the Dynamic Characteristics of a Piezohydraulic Actuator," J. Intell. Mater. Syst. Struct., vol. 16, no. 6, pp. 481–492, Jun. 2005, doi: 10.1177/1045389X05051072.

[14] J. Sirohi and I. Chopra, "Design and Development of a High Pumping Frequency Piezoelectric-Hydraulic Hybrid Actuator," J. Intell. Mater. Syst. Struct., vol. 14, no. 3, pp. 135–147, Mar. 2003, doi: 10.1177/1045389X03014003002.